Advances in Concrete Construction, *Vol. 18, No. 6 (2024) 423-433*
https://doi.org/10.12989/acc.2024.18.6.423

Influence of additional thermal and shrinkage reinforcement to reduce self-induced strain on early-age concrete

Faizal Hanif [b], Ali Awaludin* and Angga Fajar Setiawan [a]

Department of Civil & Environmental Engineering, Faculty of Engineering, Gadjah Mada University, Indonesia

(*Received July 28, 2024, Revised November 24, 2024, Accepted December 12, 2024*)

Abstract. Mass concrete deposited in restrained formwork needs special precautions to control superior heat generation, resulting in thermal expansion. High-performance concrete (HPC) requires strict water-to-cement ratio control, linked to autogenous shrinkage domination. Combining those factors with unsteady formwork support may cause significant cracking damage along the span or localized at a specific area. A special case study of existing cracking on the Jogja-Bawen Highway Project was conducted to investigate the link between emerging cracks and inadequate reinforcing steel to withstand thermal and shrinkage during early-age concrete maturing. ACI 318M-14 and AASHTO LRFD Section 5.10.8 suggested additional temperature and shrinkage reinforcement to cope with the cracking risk. Simplified full-scale finite element (FE) models with various amounts of longitudinal reinforcement and configurations were carried out to reveal improved tensile strain performance of additional reinforcing steel. This study discovered the critical role of temperature and shrinkage reinforcement as an important requirement before establishing such structural designs.

Keywords: autogenous shrinkage; finite element; mass concrete; strain gradient; thermal expansion

1. Introduction

Wide-ranging cracks were identified spreading along the pier cap after 7 days of the cast-in-place reinforced concrete portal system in Pier P87 Jogja-Bawen Highway Project, Indonesia. Experienced various cracks averaging from 0.20 mm to 0.35 mm (Fig. 1 indicated by red stripe lines), are considered critical crack width by certain standards (Basteskår *et al*. 2019). Existing cracks on primary structures may allow water and air penetration, causing internal damage such as steel corrosion and reducing adhesion between concrete and steel reinforcements (Chang *et al*. 2019). Induced internal damage caused by existing cracks will potentially compromise the durability and safety of infrastructure service life due to decreasing structural stiffness and service capacity (Hadinata *et al*. 2021, Purani 2013). Reinforcement configurations or other practical methods should serve typical non-load cracks that outstrip accepted specifications. Several investigations regarding the primary cause of cracking were associated with early-age concrete stress developed by temperature changes, elastic modulus development, shrinkage, thermal expansion, and restrained stress relaxation (Liu *et al*. 2018). Cracks occur between the developing process of tensile stress transfer until the final nominal tensile stress may exceed the tensile limit.

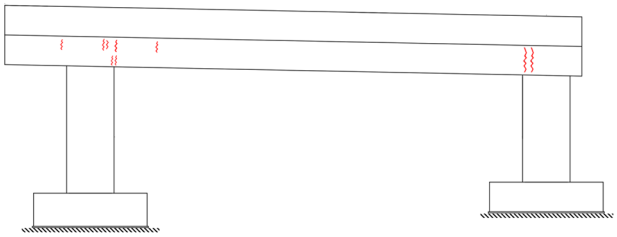

Fig. 1 Investigated crack propagation on project site (source: PT Adhi Karya documentation)

Mass concrete design in this observed pier is a fundamental principle to prioritize structural endurance to withstand required load design and economic standards. This observed structure is a compounded concrete volume with huge dimensions above 0.8 to 1.0 m, categorized as mass concrete (Bofang 2014). Considering the small tensile strength of concrete that poorly copes with significant tensile stress by thermal stresses and developed strains by volume shrinkage, mass concrete volume deposited in formworks with dimensions larger than 2.4 to 3 m needs specific precautions (ACI 207 Committee 1998). Reinforced concrete blocks as mass concrete are prone to early stages cracking caused by heat hydration development at the mass concrete core and its dissemination process to the concrete surface (Saeed *et al*. 2023). Another design aspect of the dissipation effort to reduce thermal heat needs to be investigated.

HPC utilized in this pier job mix formula obliges water reducer agents that enforce a lower water-cement ratio (Zhu *et al*. 2020), complicating construction methods modification

*Corresponding author, Ph.D.,
E-mail: ali.awaludin@ugm.ac.id
[a] Ph.D., E-mail: angga.fajar.s@ugm.ac.id
[b] M.Eng., E-mail: faizal.hanif@mail.ugm.ac.id

ISSN: 2287-5301 (Print), 2287-531X (Online)

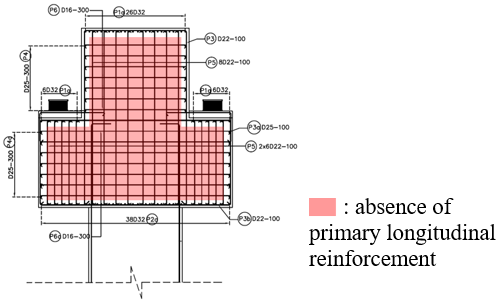

Fig. 2 Pier cap P87 (source: project's construction drawing)

and quality measures intervention. American Concrete Institute (ACI) introduced two ways to cope with mass concrete heat hydration. The first pre-cooling method suggested by ACI 207.2R-3 is reducing the initial temperature before concrete placement. The simplest method to control on-site placing temperature is adding cube ice dosage, which does not comply with the strict water-cement ratio. The second post-cooling method suggested by ACI 207.4R-93 is circulating cold water in embedded cooling pipes, which requires more space, equipment, and budget. Dense reinforcement design (Fig. 2) complicates pipe installation, and construction budget limitations may require alternating solutions to be implemented. The proposed method in this study using additional temperature and shrinkage reinforcement proposed a more affordable alternative with fewer required spaces and only required simple tools to implement.

Autogenous shrinkage leads attention to early age cracking on HPC, especially with a water-cement ratio lower than 0.40 (Wu *et al*. 2017). Autogenous shrinkage dominates the first stage of total shrinkage rather than drying shrinkage because of its low water addition. The accelerated shrinkage in restrained structures will produce tensile stress, an important cause of cracking (Tang *et al*. 2021). Extraordinary measures to minimize cracking are required to cope with the rise of thermal stress caused by hydration heat generation and volume changes resulting from autogenous shrinkage. The deposited strain energy during the concrete hardening process is greatly supported by embedded steel rebars, which provide steadiness through shear stress release. The restraining effect is also strongly influenced by elastic modulus development over time on early-age concrete, reinforcement ratio, and distance between reinforcing bars (Huang *et al*. 2017). Widely distributed reinforcement spreads tensile stress under externally restrained structures and relieves it in the form of stored strain energy to refine cracking behavior (Wang *et al*. 2023). Well-distributed reinforcement facilitates the concrete's operation in pre-peak strain capacity, resulting in delayed cracking (Sule and van Breugel 2004). The lack of central principal reinforcement is the main conjecture of experienced widespread cracks in this case study, as illustrated in Fig. 2. Temperature and shrinkage reinforcement is required in addition to principal reinforcement to minimize cracking (AASHTO 2014, ACI 318 Committee 2015). FE analysis method opened the opportunity to examine this influence of additional temperature and shrinkage reinforcement with quick interpretation results and fewer resources compared to experimental laboratory methods. Reinforced concrete elements with embedded reinforcement modeling using FE analysis is proven to be the most effective method to investigate its' behavior (Effendi 2020).

On-site early-age concrete cracking was found and investigated using the FE method by Chang *et al*. (2019) on a prestressed concrete box girder with a length of 130 m after 14 days of cast-in-site concrete. Similar study has been conducted by Liu *et al*. (2018) on cast-in-place box concrete culverts to observe formwork dismantling influence. Research investigating early-age concrete cracking on on-site structures indicated that this problem is a commonly experienced with strong links between early-age strain gradients related to concrete cracking. Mitigation regarding concrete cracking was investigated by Gribniak *et al*. (2018) and Huang *et al*. (2017), who concluded that reinforcement ratio and configuration have a shared influence on reducing cracking. However, investigations on similar cracking problems in pier caps implicating mass concrete, early-age HPC properties, and formwork deflection were still lacking.

This study suggests investigating the influence of reinforcement configurations to predict improved response and decrease the risk of early-age concrete cracking. Implementing well-distributed reinforcement would highly anticipate localized crack damage during early-age concrete hardening experienced in pier cap P87. This study presented numerical analysis research to examine the tensile strain gradient response of the original design and modified design. The benefit of temperature and shrinkage reinforcement will be presented as an alternating solution to cope with similar problems.

2. Early-age concrete parameters

Predicting apparent nominal strain involves various parameters that incorporate ideal early concrete maturing behavior to develop dynamic measures of mechanical properties. A window period between 3-12 hours is the suggested range for combined action between autogenous shrinkage and the hydration process (Niken *et al*. 2017). The maximum thermal hydration effect followed by early-age cracking characteristics exists within 72 hours (Zhu *et al*. 2020). Representative non-damage finite-element models (FEM) involving early-age concrete properties, shrinkage action, formwork deflection, and temperature loads were simulated with important time steps from 2 hours until 72 hours. Induced strain value was assessed to evaluate strain performance between models.

2.1 Modulus of elasticity

This study simulated progressive changes in early-age concrete elastic properties and aligned with formulas adopted from ACI 209R-92 and ACI 318M-08. Time-dependent compressive strength at any time was formulated as shown in Eq. (1) (ACI 209 Committee 1997). The developing compressive strength can be predicted, hence

Table 1 Time-dependent elastic modulus

Step	Time (day)	Time (hour)	f_c'(t) (MPa)	E_c (t) (MPa)
1	0.08	2	0.82	4253
2	0.42	10	3.83	9195
3	0.50	12	4.52	9992
4	1.00	24	8.25	13498
5	2.00	48	14.04	17608
6	3.00	72	18.32	20117

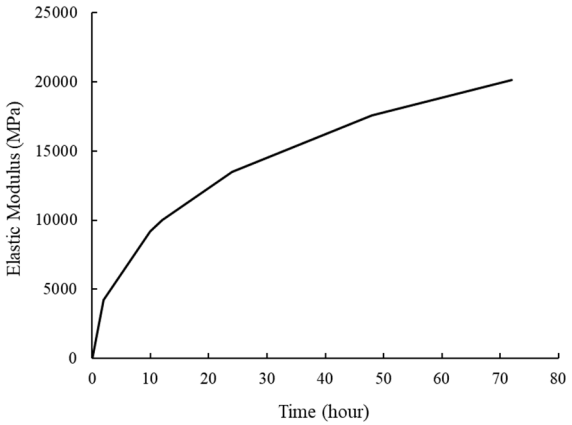

Fig. 3 Early-age elastic modulus development

the modulus of elasticity at any given time following Eq. (1) and Eq. (2) (ACI 318 Committee 2007). Combining those equations gave predictive elastic modulus, presented in Table 1 and Fig. 3. Although compressive strength and elastic modulus undergo time-dependent development, the Poisson's ratio remains relatively steady during maturity (Sideris and Manita 2004).

$$f_c'(t) = \frac{t}{a + \beta t} f_{c\,28}' \tag{1}$$

where f_c'(t) is compressive strength at any given time in MPa; t is projected concrete ages in days, a = 4.0 and β = 0.85 are curing and cement type constants; and f_c'$_{28}$ = 40 MPa is the 28-day strength target used in this project.

$$E_c(t) = 4700\sqrt{f_c'(t)} \tag{2}$$

where $E_c(t)$ is modulus elasticity related to compressive strength at any given time in MPa, and f_c'(t) is compressive strength at any given time in MPa.

2.2 Thermal expansion

Thermal stress is strongly linked to thermal expansion but not proportional to temperature fluctuations at the early age phase (Cusson and Hoogeveen 2006). The coefficient of thermal expansion (α) undergoes time-dependent changes that influence relations with thermal expansion stress. After setting time, cast-in-place concrete's α is approximately

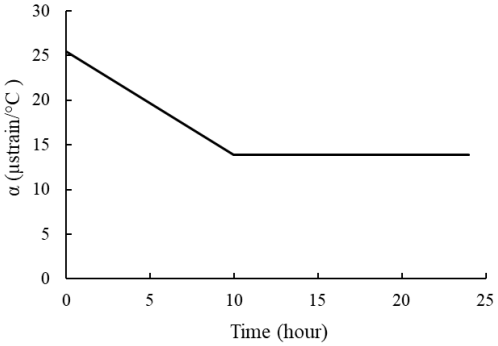

Fig. 4 Early-age α development

twice as α on the stabilized stage and relates to ambient relative humidity (Yeon *et al*. 2013). Recent research about α behavior coincided with autogenous shrinkage indicated that the greatest apparent changes in α value averaged 11.50 μstrain/°C before stabilizing normal value after 10 hours (Jeong *et al*. 2012). Based on α development approached by Jeong *et al*. (2012) and relative humidity (RH) data by the nearest local climate station at 70%-80% RH, the predictive normal value of α was determined at 13.90 μstrain/°C. Time-dependent α has been developed, as shown in Fig. 4.

The value of thermal strain due to temperature changes and α value can be derived from the thermal stress formula by Bofang (2014) and Schindler *et al*. (2002). The integrated equation to calculate the thermal strain increment for every temperature change based on those formulas is shown in Eq. (3).

$$\varepsilon_T(t) = \Delta T \times \alpha(t) \tag{3}$$

where $\varepsilon_T(t)$ is thermal expansion strain changes at time increment, ΔT is temperature increment in °C, and $\alpha(t)$ is coefficient of thermal expansion in strain/°C at time t.

2.3 Autogenous shrinkage

Shrinkage is a complex phenomenon that occurs along with hydration process. Full coverage of shrinkage behavior is an important parameter for good concrete design performance (Niken *et al*. 2021). Several autogenous shrinkage models were developed to establish good mechanisms of self-desiccation on restrained structures in relation to tensile stress or strain. Model B4 predicts average shrinkage for HPC with additives, admixtures, and a low water-to-cement ratio (Hubler *et al*. 2015). The proposed updated Model B4 is now widely implemented (Rasoolinejad *et al*. 2019) as described in Eq. (4).

$$\varepsilon_{au}(t) = k_\gamma k_s C \times t^n \tag{4}$$

where

$$k_s = (1 + 3Si_c) \times (1 + 2S_c)$$
$$C = \frac{100}{(w_c)^{2.5} + (0.1a_c)^{1.5}}$$
$$n = (1.2 - 0.1a_c) + [(-0.14 + 0.005a_c)\, ln\, C]$$

t is the respective time in days; $\varepsilon_{au}(t)$ is autogenous

Table 2 Time-dependent autogenous shrinkage

Step	Time (day)	Time (hour)	ε_{au} (t) (μstrain)	$\Delta\varepsilon_{au}$ (t) (μstrain)	$\Delta\varepsilon_{au}$ (strain)
1	0.08	2	732.28	0	0
2	0.42	10	795.75	63.47	3.66e-5
3	0.50	12	803.28	7.53	4.10e-5
4	1.00	24	832.56	29.28	5.79e-5
5	2.00	48	862.90	30.35	7.54e-5
6	3.00	72	881.17	18.26	8.60e-5

Table 3 Time-dependent adiabatic temperature rise

Step	Time (day)	Time (hour)	ΔT (°C)	T (°C)
1	0.08	2	0	37.78
2	0.42	10	8.14	45.92
3	0.50	12	2.04	47.96
4	1.00	24	3.25	51.20
5	2.00	48	1.93	53.14
6	3.00	72	0.69	53.83

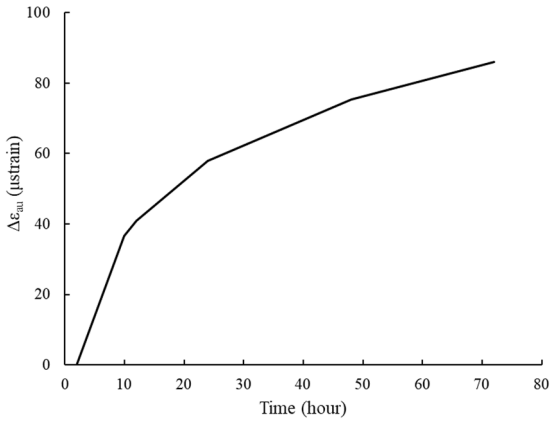

Fig. 5 Single-axis autogenous shrinkage strain development

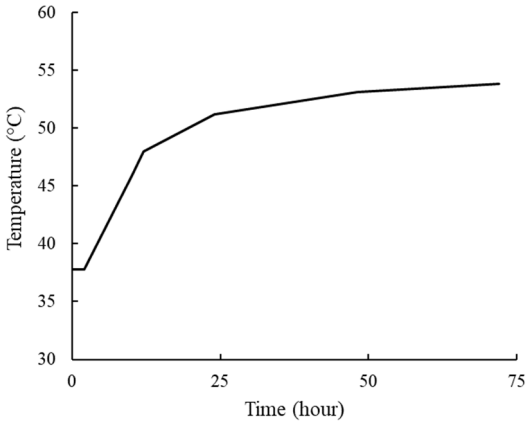

Fig. 6 Temperature rise development

shrinkage strain at any time; k_γ = 1 is the cement type parameter for ordinary Portland cement; k_s is coefficient of silica fume and slag, Si_c = 21% for silica-to-cement ratio, S_c = 65% for slag-to-cement ratio; w_c = 0.32 is water-to-cement ratio; a_c = 5.37 is aggregate-to-cement ratio referred to concrete job mix.

Calculated autogenous shrinkage strains respective to time must be adjusted with the designated initial setting time at the start of measurement. Change of autogenous shrinkage strain for each time step ($\Delta\varepsilon_{au}$) were calculated by subtracting each of $\varepsilon_{au}(t)$ by initial autogenous shrinkage on 1st time step. Some references suggested that the initial setting time ranged from 100 minutes to 150 minutes for field conditions before the final setting time (Pinto and Hover 1999, Schindler *et al*. 2002). An initial setting time of 2 hours was used in this study as a starting point for autogenous shrinkage strain measurement. The calculated volumetric strain based on updated Model B4 was then simplified to a single-axis strain, as presented in Table 2 and Fig. 5.

2.4 Temperature rise

Heat generation has a crucial role before all concrete properties are fully developed. Temperature rise prediction approached by placing temperatures factors was utilized in this study to set the temperature rise between time steps. The placing temperature was assumed to be 100°F or equal to 37.78°C as a basic determination to recall data from graph-based reference (ACI 207 Committee 2007). The adiabatic thermal gradient is the temperature changes through sections specific to a temperature difference between the internal and external parts. Generalized temperature changes were implemented as constant throughout all regions so that the calculated temperature rise was multiplied by half. The generalized temperature rise for each incremental step is presented in Table 3 and Fig. 6, which is equal to a total adiabatic temperature rise of T = 32.10°C.

2.4 Degree of restraint

The FE model in this study implemented formwork deflection behavior because formwork is an example of an external restraint that affects nominal thermal stress proportionally to the degree of restraint constant (Mehta and Monteiro 2014). The restraint factor is also one of the causes of cracking, which hinders the structural ability to release volumetric changes (Brown *et al*. 2001). Inaccurate restraint models may cause an imprecise response between total induced stress and strain translation.

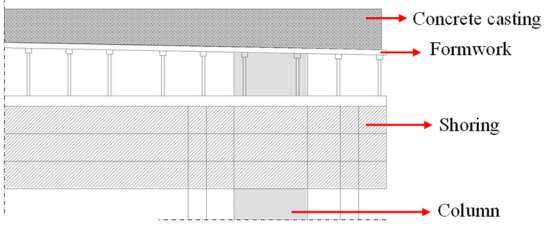

Fig. 7 On-site shoring system to support formwork

Table 4 Time-dependent restraint releases

Step	Time (day)	Time (hour)	Restraint release (mm)
1	0.08	2	0.0
2	0.42	10	0.0
3	0.50	12	5.0
4	1.00	24	10.0
5	2.00	48	10.0
6	3.00	72	10.0

3. Finite element modelling

FE analysis was performed in this study using a standard solver of ABAQUS with additional Fortran USDFLD and UEXPAN subroutines. Concrete elastic modulus (E_c) defined as time dependent functions following Table 1, while its isotropic thermal expansion rate (α) defined as time dependent functions following Fig. 4. Eq. (5) stated the volumetric strain load (ε_{tot}) expressed by thermal expansion (ε_T) as formulated on Eq. (3), then subtracted by autogenous shrinkage ($\Delta\varepsilon_{au}$) as prescribed in Table 2.

$$\varepsilon_{tot} = \varepsilon_T(t) - \Delta\varepsilon_{au} \quad (5)$$

where ε_{tot} is the total effective volumetric strain load at time increment, $\varepsilon_T(t)$ is thermal expansion strain, and $\Delta\varepsilon_{au}$ is autogenous shrinkage strain changes.

Time dependent loading was defined as temperature changes (ΔT) as presented in Table 3. Temperature load worked as concrete expansion behavior within thermal expansion strain function (ε_T). All material responses caused by temperature loading were defined as linear elastic to engage non-damage behavior with strain limit as a cracking indicator. Restraint release mechanisms were simulated as boundary condition change on formwork support as stated in Table 4. The summary of early age simulations for each time step is presented in Table 5.

3.1 Compiling Fortran user subroutines

This research aims to implement and incorporate early-age parameters in FE modeling. Most FE programs don't provide a user-friendly interface to input time-dependent parameters, so Fortran subroutines were developed to expand the ABAQUS software capabilities. All parameters and functions were incorporated by Fortran subroutines directly into the ABAQUS standard solver in respective order (Ahmad Rafsanjani 2010), as presented in Fig. 8.

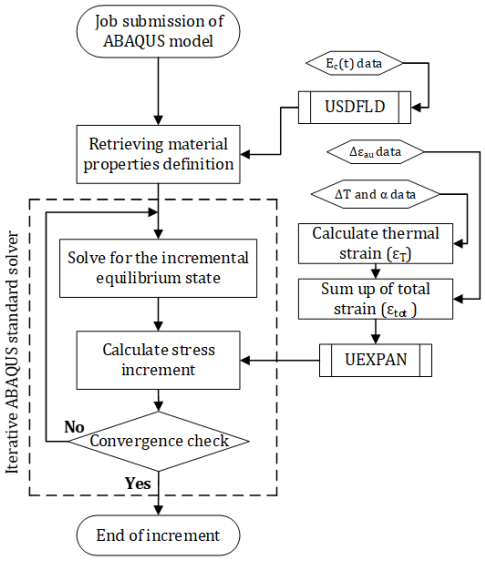

Fig. 8 Workflow of Fortran subroutines linked to ABAQUS iterative solver

The step-by-step iterative method requires numerical time integration to complete an integrated constitutive relation. The UEXPAN user subroutine was utilized to calculate incremental total strain as stated in Eq. (5), which carried additional codes to calculate thermal strain and defined autogenous strain. Concrete elastic modulus development was defined in predefined fields aligned with each time step in USDFLD subroutines. Combined USDFLD and UEXPAN subroutines are implemented as an alternative method to implement equivalent age maturity. Linking the ABAQUS standard solver with Fortran subroutines enables a numerical solution for each step and subsequent increments (Zhu *et al*. 2020).

3.2 Representative FE model variations

Summary of ACI 318M-14 and AASHTO LRFD Section 5.10.8 specifications for gross sectional area ratio

Table 5 Summary of time-dependent early age properties

	Step	Time (day)	Time (hour)	T (°C)	E_c (t) (MPa)	α (strain/°C)	$\Delta\varepsilon_{au}$ (strain)	Restraint release (mm)
0	Initial	-	-	37.78	-	2.54e-5	-	-
1	t1-2H	0.08	2	37.78	4253	*linear*	0	0.0
2	t2-10H	0.42	10	45.92	9195		3.66e-5	0.0
3	t3-12H	0.50	12	47.96	9992	1.39e-5	4.10e-5	5.0
4	t4-24H	1.00	24	51.20	13498	1.39e-5	5.79e-5	10.0
5	t5-48H	2.00	48	53.14	17608	1.39e-5	7.54e-5	10.0
6	t6-72H	3.00	72	53.83	20117	1.39e-5	8.60e-5	10.0

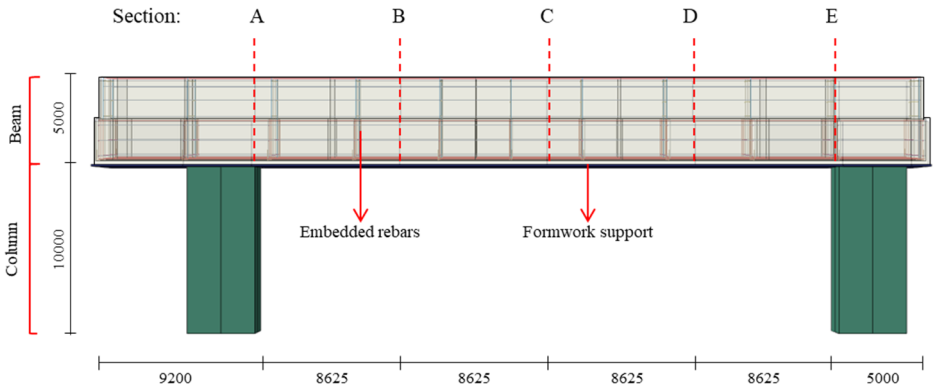

Fig. 9 Representation of simplified 3D ABAQUS model (dimensions in mm)

Table 6 Specifications for temperature and shrinkage reinforcement

Specification	A_s (m^2/m)	S (mm)
ACI 318M-14	0.014-0.020	450.0
AASHTO LRFD 5.10.8	0.013-0.023	304.8

three-dimensional (3D) model was modeled in ABAQUS (Fig. 9) using two element types of concrete and steel. The assembled sections were discretized into C3D8R for concrete 3D stress analysis and T3D2 for steel 3D truss elements. The mesh assignment number of 250 mm for the pier cap was determined as a balanced mess assignment based on acceptable convergence and limited computational resources. General constraints are defined as steel rebars embedded into pier cap sections and beam-columns as tie constraints. A total of 2 original models and 3 updated model variations were proposed with crisscrossed D16 steel bars, as stated in Table 7.

3.3 Strain limit evaluation

The initial cracking point is between 0.00015 and 0.00025 of the maximum tensile strain limits (Shen *et al.* 2019), defined as concrete ultimate damage capacity. The simulation model used in this study will observe a tensile gradient limited to a non-damage model. Based on the strain result, the tensile strain gradient will be observed to inspect strain intensity transfer flow and configurated reinforcements response as a tensile strain pattern. Based on Eq. (2) and Eq. (6) (ACI 318 Committee 2007), simple calculation by dividing tensile strength (f_{ct}) and elastic modulus (E_c) would define the strain limit value indicated by the logarithmic strain of 0.00012 and be used as the strain gradient limit operating in non-damage models in this study.

$$f_{ct}(t) = 0.56\sqrt{f_c'(t)} \tag{6}$$

where $f_{ct}(t)$ = tensile strength at any given time in MPa, and $f_c'(t)$ is compressive strength at any given time in MPa.

Indication of crack development parameters on ABAQUS CAE can be derived from damage model, plastic strain, or logarithmic strain (Jumaa and Yousif 2019).

Table 7 Summary of reinforcement configurations as research variables

Reinforcement configurations	Remarks
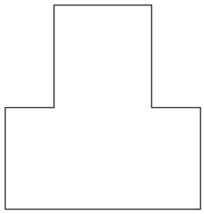	Model A Concrete only
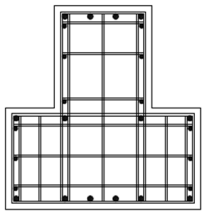	Model B Unmodified reinforcement
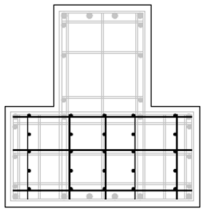	Model C-1 Modified with additional reinforcement (─ shaped) As = 0.017 m^2/m S = 450 mm
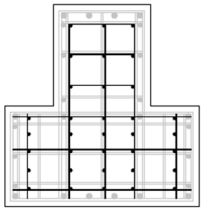	Model C-2 Modified with additional reinforcement (⊥ shaped) As = 0.023 m^2/m S = 450 mm
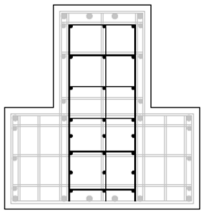	Model C-3 Modified with additional reinforcement (I shaped) As = 0.016 m^2/m S = 450 mm

Logarithmic strain measure is widely used in a constitutive model that operates on the volumetric strain model (Latorre and Montáns 2014). Logarithmic strains on the Z-axis value (LE33) will be observed to obtain true engineering strain.

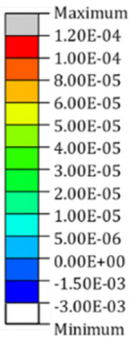

Fig. 10 Color gradation scale for strain gradients

The strain flow pattern is shown in red as the nominal tensile strain limit of 0.00012 and in gray area that has experienced strain intensity transfer, as illustrated by Fig. 10.

4. Intact design strain behaviour

4.1 Verification by on-site crack data

A proper model to monitor stress evolution can be implemented using an integration point level to handle cracking and strain concentration on an iterative step. During simultaneous strain limit flow computation, each cracking strain increment is processed as cumulative updates to the cracking strain limit flow (Feenstra and De Borst 1996). The non-damage model proceeds gradual cracking and finalize damaged risk regions represented by a banded zonation (Geers *et al*. 1998). Based on the on-site crack data (Fig. 11), the surroundings of section A area suffered more visible crack appearances than other sections, indicating localized strain concentrated deformation occurrences. Simulated FE can describe deformation verification result to express localized damaged regions.

The step-by-step results confirmed that strain limit flow is localized towards Section A, expressed by the strain

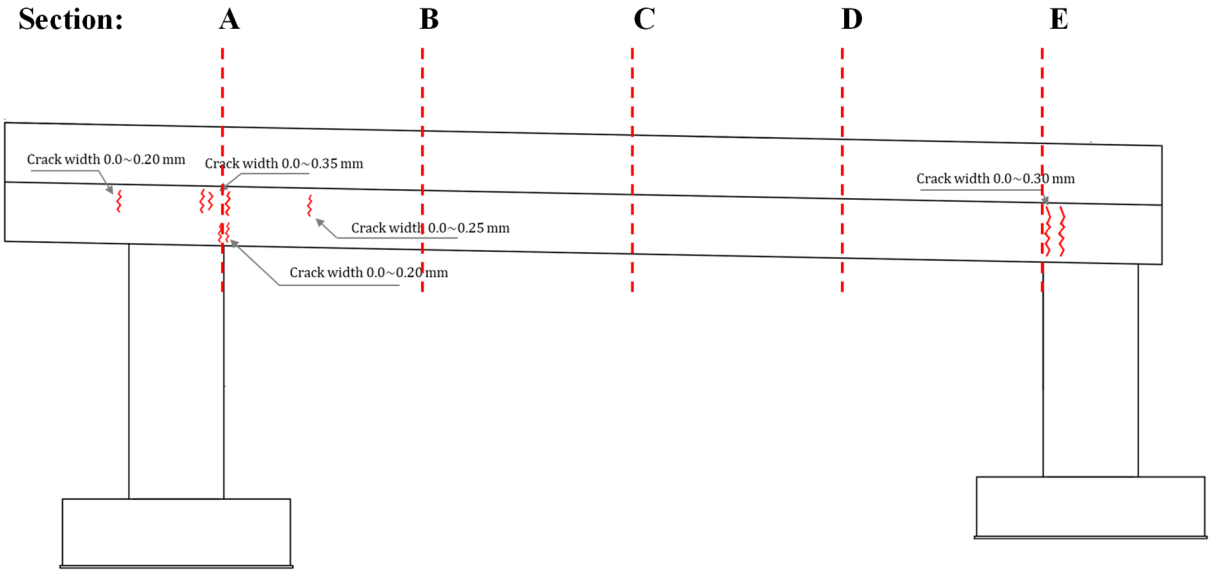

Fig. 11 Crack documentation of the entire span (source: PT Adhi Karya documentation)

Table 8 Strain gradient flows of every major time step (Model B)

Time (hour)	Strain gradient	Time (hour)	Strain gradient
10	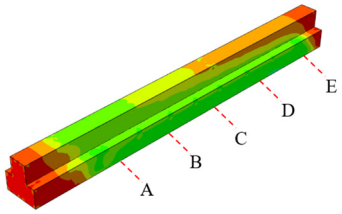	24	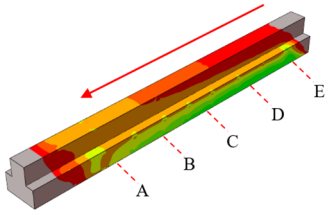
48	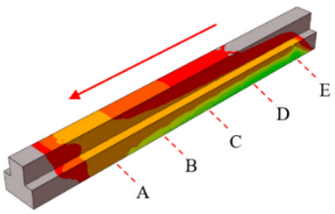	72	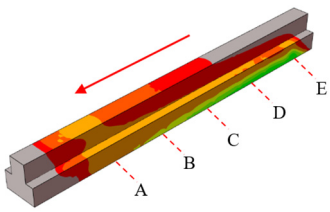

Table 9 Sectional strain gradient comparison of Model A and Model B

Section	Model A	Model B
A	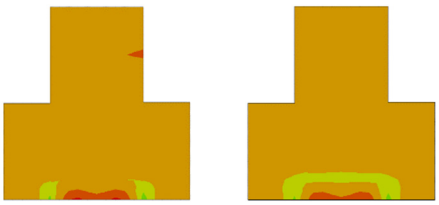	
B	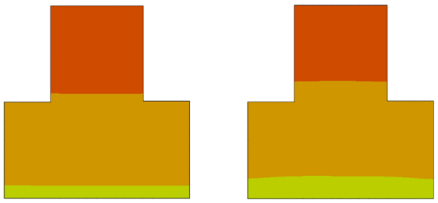	
C	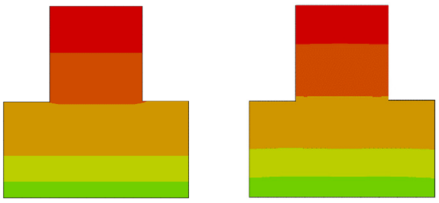	
D	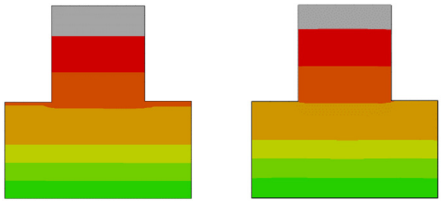	
E	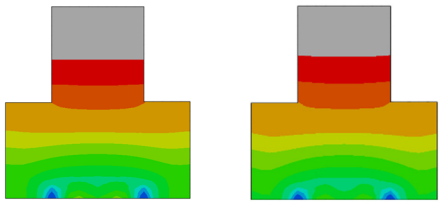	

gradient limit flow of Model B, as shown in Table 8. Reinforced concrete manifests visible macroscopic cracking which known as strain softening behavior (de Borst and Pamin 1996). Based on previous studies by Liu *et al.* (2018), Chang *et al.* (2019), and Gribniak *et al.* (2018) showed that strain intensity concentration aligned well with major macroscopic cracking zonation as the manifestation of strain softening behavior. On-site crack data indicates strain softening behavior localized around Section A, which is conformable with accumulated strain intensity flows towards the same direction as demonstrated by FE analysis. The simulation result indicated that strain intensity flows directed to Section A and caused localized crack damage.

4.2 Behaviour of unmodified reinforcement

Reinforcement model in this study neglected the stress transfer capability between concrete and reinforcement through bonding action. Modeling bond action requires complex parameters, heavy computational resources, and smaller iterative steps for a full-scale model. Therefore, all tension compression is assumed to be carried by the transversal and longitudinal reinforcement truss mechanism. The representation of physical distributed strain in previously mentioned method can only be assessed using approximate manner (Gribniak *et al.* 2018). An approximate approach was expected to provide underestimated performance and better crack demonstration to evaluate stress transfer and distribution.

Direct comparison of the sectional strain gradient of Model A (concrete only) versus Model B (original reinforcement) demonstrated minimal or almost insignificant performance for original design (Table 9). Similar strain gradients through Model A and Model B sections allegedly indicated that the original reinforcement design wasn't optimized for thermal and shrinkage strain. Areas beyond the tensile strain limit hinted by grey areas and borders between colors, expressed that strain intensity flow to the bottom section of the pier cap. Additional reinforcement for Model C-1, C-2, and C-3 was prioritized and placed at the bottom of the section based on that observation. Different strain gradient patterns between Section A and E demonstrated unbalanced strain intensity flow, indicating that strain intensity couldn't be fairly transferred to the neighboring column.

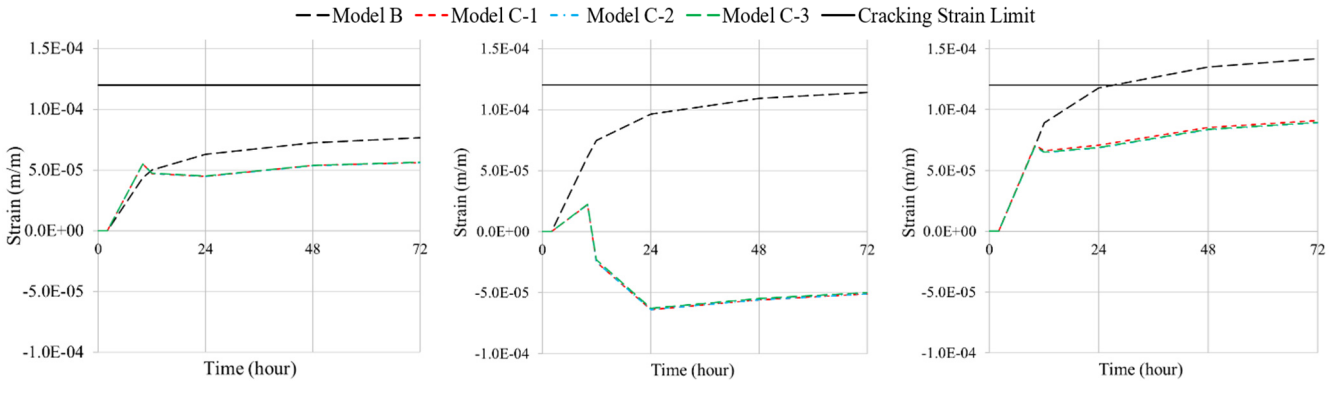

(a) Section A (b) Section C (c) Section E

Fig. 12 Time-dependent strain history of Model B and Model C-1, C-2, C-3

Table 10 Strain gradient flows of every major time step (Model C-1, C-2, and C-3)

Time (hour)	Strain gradient		
	Model C-1	Model C-2	Model C-3
10	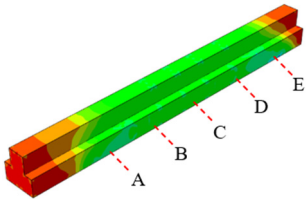	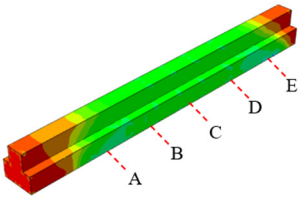	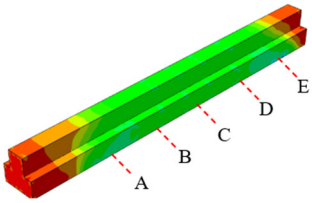
24	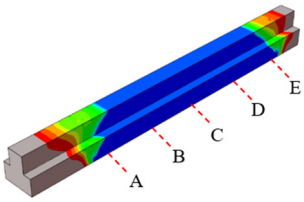	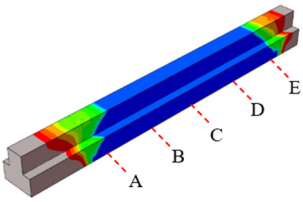	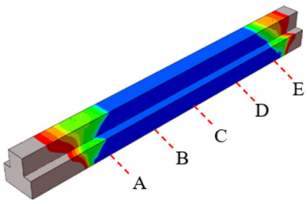
48	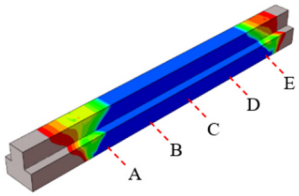	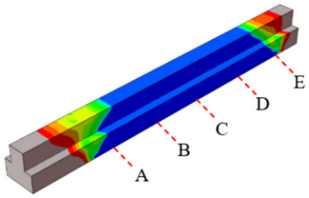	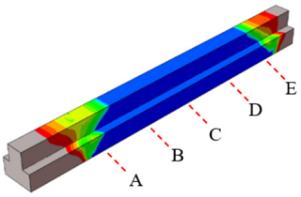

5. Significance of modified reinforcement

5.1 Strain gradient shifts

The concrete tensile capacity is much lower than its compressive capacity, so steel reinforcement is utilized to resist tension, distribute cracks, limit crack width, and protect against brittle failure. Flexural expansion behavior caused by the thermal and shrinkage effect is carried by a shear force-resisting system of longitudinal and transversal reinforcement to protect a structure from visible crack growth (Słowik 2019). Updated reinforcement design showed better tensile strain resisting performance, as shown by drastic strain response changes on the mid-span (Section C) and strain reduction on the end-span (Sections A and E), as shown in Fig. 12. Model C-1, C-2, and C-3 which are modified with additional reinforcement showed that by adding thermal and shrinkage reinforcement can greatly reduce strain on early-age concrete development. Overall, tensile strain performance was greatly improved, and emerging cracking risks could be scaled down.

The inverted strain response of Model B versus Model C-1, C-2, and C-3 after restraint release boundary condition was initiated at the 12H step showed that Model C-1, C-2, and C-3 responds better to stress release mechanisms. Such a mentioned ability is very important as on-site formwork deformation is inevitable in construction sites.

Model C-1, C-2, and C-3 have a smaller area performing under tension strain as indicated by the lesser red contour versus Model B. Comparing mid-span tension strain indicated by the red contour on Model B (Table 8), more uniform compression strain distribution was observed by blue contour on Model C-1, C-2, and C-3 (Table 10). Although the grey contour indicating an area beyond the tensile strain limit value still exists on Model C-1, C-2, and C-3, overall outstripped tension strain gradient flow was greatly reduced. Avoiding unbalanced strain intensity flow is important because Model B cannot fairly distribute strain and accumulated strain concentration towards Section A. Well-distributed strain limit flows on Model C-1, C-2, and C-3 prevent localized strain softening behavior resulting in less crack damages.

5.2 Reinforcement configuration

The original reinforcement design (Model B) is considered to have inadequate longitudinal reinforcement despite having dense transversal reinforcement. Closely tied longitudinal and transversal bars work jointly to govern the lateral dilation and allowing better core confinement system (Hernández-Montes *et al*. 2004). Model C-1, C-2, and C-3 showed better core confinement management and lowered lateral dilation by having better strain intensity distribution (Table 11). Hence confirming that ACI 318M-14 and AASHTO LRFD Section 5.10.8 regulation may align with concrete core confining management.

Comparing sectional strain gradient of Model B (Table 9) versus Model C-1, C-2, and C-3 (Table 11) demonstrated lower strain gradient below the strain limit throughout all sections which indicated by the absence of grey or white contour color. Further confining reinforcement ratio study should be conducted since Models C-1, C-2, and C-3 had similar or almost equal performance with slight nominal strain limit capacity differences, as shown in Table 11.

The outlined study result (Fig. 13) shows that any configured additional reinforcement could reduce up to 79% for mid-span and 26%-36% for end-span in terms of maximum tensile strain gradient compared to unmodified

Table 11 Sectional strain gradient comparison of Model C-1, C-2, and C-3

Section	Model C-1	Model C-2	Model C-3
A	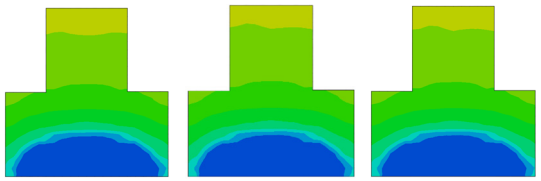		
B	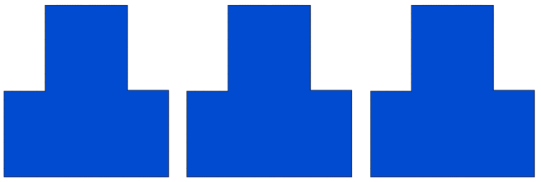		
C	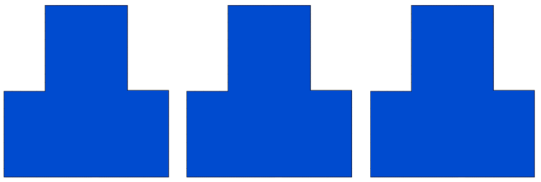		
D	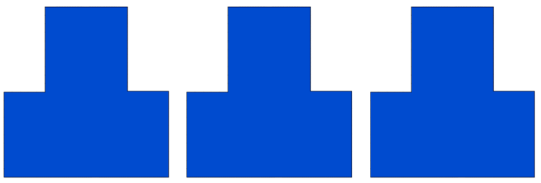		
E	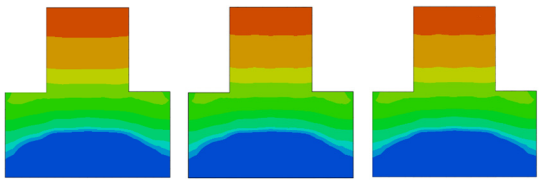		

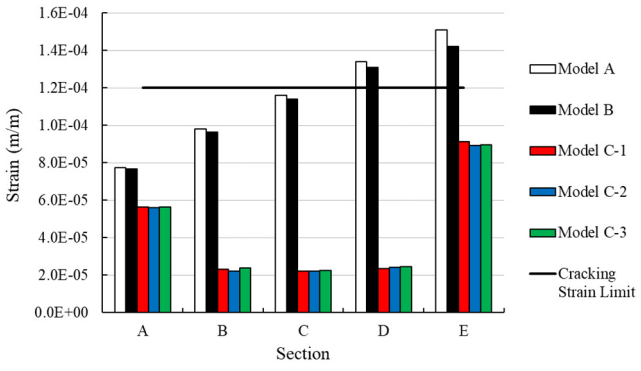

Fig. 13 Overall strain limit performance

reinforcement design. Overall performance of additional reinforcement configuration could minimize sectional tensile strain below the strain limit level.

6. Conclusions

The behavior of a high-performance reinforced concrete portal system with a strict water-to-cement ratio on the Pier P87 Jogja-Bawen Highway Project involves many early-age properties that have been considered in FE modeling in this study. On-site crack data have validated the model simulation using ABAQUS and Fortran subroutines based on localized strain softening areas. The strain behavior results of unmodified design (Model B) compared to concrete only (Model A) verified that crack occurrences on pier cap P87 were caused by inadequate reinforcement capability to withstand thermal expansion and autogenous shrinkage. Improved sectional design by adding thermal and shrinkage reinforcement (Model C-1, C-2, and C-3) based on ACI 318M-14 and AASHTO LRFD Section 5.10.8 indicated significant tension strain reduction in response to early-age HPC properties. Updated reinforcement designs had lowered tensile strain on the end-span (Sections A and E) and converted tensile strain into compressive strain on the mid-span (Sections B, C, and D). Pre-design reviews involving factors of concrete job mix, mass concrete criteria, and formwork support are important checks to consider the possibility of crack occurrences. This study has demonstrated that consideration of additional thermal and shrinkage reinforcement can be an alternate solution to minimize crack damage.

Acknowledgments

The authors would like to thank PT Adhi Karya (Persero), especially for the Jogja-Bawen Tollways project team and the support of Gadjah-Mada University staff. We also want to thank Mr. Teddy Theryo (Florida Department of Transportation) and Mr. Ueda Tamon (Former Professor at Hokkaido University) for their advice on improving this writing.

References

AASHTO (2014), American Association of State Highway and Transportation Officials: LRFD Bridge Design Specifications.

ACI 207 Committee (1998), ACI 207.4R-93 Cooling and insulating systems for mass concrete. In ACI 207.4 R-93.

ACI 207 Committee (2007), ACI 207.2R-07 Report on Thermal and Volume Change Effects on Cracking of Mass Concrete.

ACI 209 Committee (1997), ACI 209R-92 Prediction of Creep, Shrinkage, and Temperature Effects in Concrete Structures.

ACI 318 Committee (2007), ACI 318M-08 Building Code Requirements for Structural Concrete.

ACI 318 Committee (2015), ACI 318M-14 Building Code Requirements for Structural Concrete.

Ahmad Rafsanjani (2010), Writing User Subroutines with ABAQUS. https://Imechanica.Org/Node/7576

Basteskår, M., Engen, M., Kanstad, T. and Fosså, K.T. (2019), "A review of literature and code requirements for the crack width limitations for design of concrete structures in serviceability limit states", *Struct. Concrete*, **20**(2), 678-688. https://doi.org/10.1002/suco.201800183

Bofang, Z. (2014), *Thermal Stresses and Temperature Control of Mass Concrete*, Elsevier. https://doi.org/10.1016/C2012-0-06038-3

Brown, M.D., Sellers, G.D., Folliard, K.J. and Fowler, D.W. (2001), "Restrained shrinkage cracking of concrete bridge decks: State-of-the-Art Review". https://api.semanticscholar.org/CorpusID:53575018

Chang, S., Yang, M., Sun, Y. and Liu, K. (2019), "Calculation Method of Early-Age Crack Width in Reinforced Concrete Bridge through a Nonlinear FEA Model", *KSCE J. Civil Eng.*, **23**(7), 3088-3096. https://doi.org/10.1007/s12205-019-2129-0

Cusson, D. and Hoogeveen, T. (2006), "Measuring early-age coefficient of thermal expansion in high-performance concrete", In: *International RILEM Conference on Volume Changes of Hardening Concrete: Testing and Mitigation*, pp. 321-330.

De Borst, R. and Pamin, J. (1996), "Gradient plasticity in numerical simulation of concrete cracking", *Eur. J. Mech. A-Solids*, **15**, 295-320. https://api.semanticscholar.org/CorpusID:120125026

Effendi, M.K. (2020), "Non-linear finite element analysis of flexural reinforced concrete beam using embedded reinforcement modeling", *J. Civil Eng. Forum*, **6**(3), 271. https://doi.org/10.22146/jcef.55960

Feenstra, P.H. and De Borst, R. (1996), "A composite plasticity model for concrete", *Int. J. Solids Struct.*, **33**(5), 707-730. https://doi.org/10.1016/0020-7683(95)00060-N

Geers, M.G.D., De Borst, R., Brekelmans, W.A.M. and Peerlings, R. (1998), "Strain-based transient-gradient damage model for failure analyses", *Comput. Methods Appl. Mech. Eng.*, **160**(1-2), 133-153. https://doi.org/10.1016/S0045-7825(98)80011-X

Gribniak, V., Jakubovskis, R., Rimkus, A., Ng, P.-L. and Hui, D. (2018), "Experimental and numerical analysis of strain gradient in tensile concrete prisms reinforced with multiple bars", *Constr. Build. Mater.*, **187**, 572-583. https://doi.org/10.1016/j.conbuildmat.2018.07.152

Hadinata, P.N., Simanta, D., Eddy, L. and Nagai, K. (2021), "Crack Detection on Concrete Surfaces Using Deep Encoder-Decoder Convolutional Neural Network: A Comparison Study Between U-Net and DeepLabV3+", *J. Civil Eng. Forum*, **7**(3), 323. https://doi.org/10.22146/jcef.65288

Hernández-Montes, E., Aschheim, M. and Gil-Martín, L.M. (2004), "Impact of optimal longitudinal reinforcement on the curvature ductility capacity of reinforced concrete column sections", *Magaz. Concrete Res.*, **56**(9), 499-512. https://doi.org/10.1680/macr.2004.56.9.499

Huang, L., Hua, J., Kang, M. and Zhang, A. (2017), "Influence of reinforcement configuration on the shrinkage and cracking potential of high-performance concrete", *Constr. Build. Mater.*, **140**, 20-30. https://doi.org/10.1016/j.conbuildmat.2017.02.074

Hubler, M.H., Wendner, R. and Bažant, Z.P. (2015), "Statistical justification of Model B4 for drying and autogenous shrinkage of concrete and comparisons to other models", *Mater. Struct.*, **48**(4), 797-814. https://doi.org/10.1617/s11527-014-0516-z

Jeong, J.-H., Zollinger, D.G., Lim, J.-S. and Park, J.-Y. (2012), "Age and moisture effects on thermal expansion of concrete pavement slabs", *J. Mater. Civil Eng.*, **24**(1), 8-15. https://doi.org/10.1061/(ASCE)MT.1943-5533.0000342

Jumaa, G.B. and Yousif, A.R. (2019), "Numerical modeling of size effect in shear strength of FRP-reinforced concrete beams", *Structures*, **20**, 237-254. https://doi.org/10.1016/j.istruc.2019.04.008

Latorre, M. and Montáns, F.J. (2014), "On the interpretation of the logarithmic strain tensor in an arbitrary system of representation", *Int. J. Solids Struct.*, **51**(7-8), 1507-1515. https://doi.org/10.1016/j.ijsolstr.2013.12.041

Liu, Y., Schindler, A.K. and Davidson, J.S. (2018), "Finite-Element Modeling and Analysis of Early-Age Cracking Risk of Cast-In-Place Concrete Culverts", *Transport. Res. Record: J. Transport. Res. Board*, **2672**(27), 24-36. https://doi.org/10.1177/0361198118774157

Mehta, P.K. and Monteiro, P.J.M. (2014), *Concrete: Microstructure, Properties, and Materials* (4th Edition), McGraw-Hill Education. https://www.accessengineeringlibrary.com/content/book/9780071797870

Niken, C., Tjahjono, E. and Supartono, F. (2017), "Long-term deformation of beam and column of high performance concrete", *Int. J. Technol.*, **8**(5), 811. https://doi.org/10.14716/ijtech.v8i5.863

Niken, C., Tjahjono, E. and Supartono, F. (2021), "Rheological Model of Concrete Shrinkage", *Int. J. Technol.*, **12**(1), 217. https://doi.org/10.14716/ijtech.v12i1.2818

Pinto, R. and Hover, K. (1999), "Application of maturity approach to setting times", *ACI Mater. J.*, **96**(6), 686-691. https://doi.org/10.14359/795

Purani, D. (2013), *Incorporating shrinkage effects in FE Modeling of Prestressed Concrete Bridge*, Rutgers The State University of New Jersey, School of Graduate Studies.

Rasoolinejad, M., Rahimi-Aghdam, S. and Bažant, Z.P. (2019), "Prediction of autogenous shrinkage in concrete from material composition or strength calibrated by a large database, as update to model B4", *Mater. Struct.*, **52**(2), 33. https://doi.org/10.1617/s11527-019-1331-3

Saeed, M.K., Rahman, M.K., Alfawzan, M., Basha, S. and Dahish, H.A. (2023), "Recycling of date kernel powder (DKP) in mass concrete for mitigating heat generation and risk of cracking at an early age", *Constr. Build. Mater.*, **376**, 131033. https://doi.org/10.1016/j.conbuildmat.2023.131033

Schindler, A.K., Dossey, T. and McCullough, B.F. (2002), "Temperature control during construction to improve the long term performance of Portland cement concrete pavements", No. FHWA/TX-05/0-1700-2.

Shen, Q., Chen, W., Liu, C., Zou, W. and Pan, L. (2019), "The tensile strength and damage characteristic of two types of concrete and their interface", *Materials*, **13**(1), 16. https://doi.org/10.3390/ma13010016

Sideris, K.K. and Manita, P. (2004), "Estimation of ultimate modulus of elasticity and Poisson ratio of normal concrete", *Cement Concrete Compos.*, **26**(6), 623-631. https://doi.org/10.1016/S0958-9465(03)00084-2

Słowik, M. (2019), "The analysis of failure in concrete and reinforced concrete beams with different reinforcement ratio", *Arch. Appl. Mech.*, **89**(5), 885-895. https://doi.org/10.1007/s00419-018-1476-5

Sule, M. and van Breugel, K. (2004), "The effect of reinforcement on early-age cracking due to autogenous shrinkage and thermal effects", *Cement Concrete Compos.*, **26**(5), 581-587. https://doi.org/10.1016/S0958-9465(03)00078-7

Tang, S., Huang, D. and He, Z. (2021), "A review of autogenous shrinkage models of concrete", *J. Build. Eng.*, **44**, 103412. https://doi.org/10.1016/j.jobe.2021.103412

Wang, H., Liu, Y., Hu, Z., Li, H., Yao, T. and Liu, J. (2023), "Influencing aspects and mechanisms of steel bar reinforcement on shrinkage and cracking of cement-based materials: A review", *J. Build. Eng.*, **77**, 107476. https://doi.org/10.1016/j.jobe.2023.107476

Wu, L., Farzadnia, N., Shi, C., Zhang, Z. and Wang, H. (2017), "Autogenous shrinkage of high performance concrete: A review", *Constr. Build. Mater.*, **149**, 62-75. https://doi.org/10.1016/j.conbuildmat.2017.05.064

Yeon, J.H., Choi, S. and Won, M.C. (2013), "In situ measurement of coefficient of thermal expansion in hardening concrete and its effect on thermal stress development", *Constr. Build. Mater.*, **38**, 306-315. https://doi.org/10.1016/j.conbuildmat.2012.07.111

Zhu, L., Wang, J.-J., Li, X., Zhao, G.-Y. and Huo, X.-J. (2020), "Experimental and numerical study on creep and shrinkage effects of ultra high-performance concrete beam", *Compos. Part B: Eng.*, **184**, 107713. https://doi.org/10.1016/j.compositesb.2019.107713